iScience

CellPress
OPEN ACCESS

Article

Helical peptides with disordered regions for measles viruses provide new generalized insights into fusion inhibitors

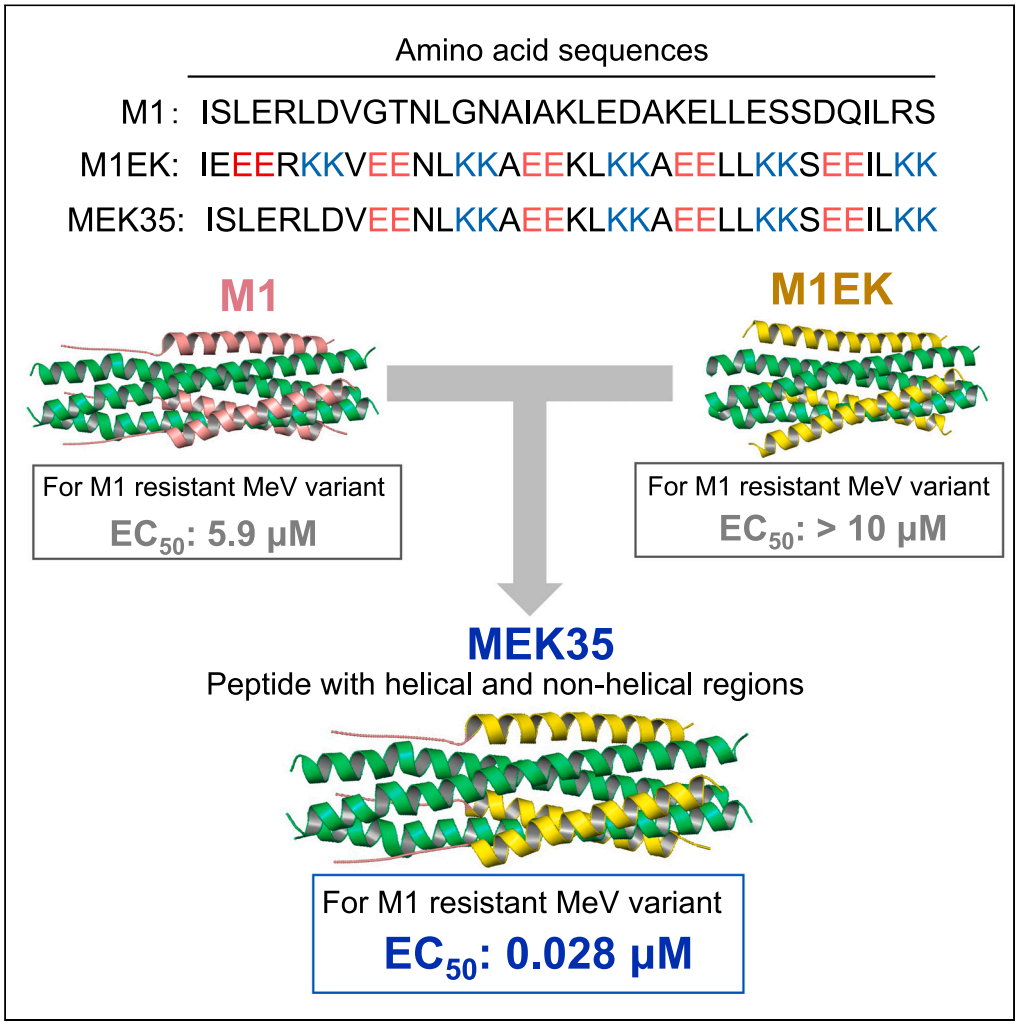

Kazushige Hirata, Aoi Takahara, Satoshi Suzuki, ..., Hironori Hayashi, Shinya Oishi, Eiichi N. Kodama

hhayashi@med.tohoku.ac.jp

Highlights

Peptide with disordered and helical regions inhibits drug-resistant measles variants

Hirata et al., iScience 27, 108961
February 16, 2024
https://doi.org/10.1016/j.isci.2024.108961

iScience

CellPress
OPEN ACCESS

Article

Helical peptides with disordered regions for measles viruses provide new generalized insights into fusion inhibitors

Kazushige Hirata,[1,2] Aoi Takahara,[3] Satoshi Suzuki,[1] Shumei Murakami,[4,5] Kumi Kawaji,[5] Akie Nishiyama,[1] Mina Sasano,[5] Mariko Shoji-Ueno,[1] Emiko Usui,[5] Kazutaka Murayama,[6] Hironori Hayashi,[4,5,9,*] Shinya Oishi,[3,7] and Eiichi N. Kodama[4,5,8]

SUMMARY

Despite effective vaccines, measles virus (MeV) outbreaks occur sporadically. Therefore, developing anti-MeV agents remains important for suppressing MeV infections. We previously designed peptide-based MeV fusion inhibitors, M1 and M2, that target MeV class I fusion protein (F protein). Here, we developed a novel fusion inhibitor, MEK35, that exerts potent activity against M1/M2-resistant MeV variants. Comparing MEK35 to M1 derivatives revealed that combining disordered and helical elements was essential for overcoming M1/M2 resistance. Moreover, we propose a three-step antiviral process for peptide-based fusion inhibitors: (i) disordered peptides interact with F protein; (ii) the peptides adopt a partial helical conformation and bind to F protein through hydrophobic interactions; and (iii) subsequent interactions involving the disordered region of the peptides afford a peptide-F protein with a high-affinity peptide-F protein interaction. An M1-resistant substitution blocks the second step. These results should aid the development of novel viral fusion inhibitors targeting class I F protein.

INTRODUCTION

Measles virus (MeV) is an enveloped virus with a negative-strand RNA genome that belongs to the genus Morbillivirus and the family Paramyxoviridae. The two-dose MeV vaccine has reduced the number of measles patients globally. Notably, the MeV vaccine has been used successfully to achieve regional elimination of measles in North and South America.[1] Nonetheless, a herd immunity of ~95% is required to prevent measles outbreaks because of the extremely high infectivity of MeV (primary basic reproduction number (R_0) of measles = 12–18), which is 2–3 times higher than the R_0 of patients infected with the novel coronavirus, severe acute respiratory syndrome coronavirus 2 (SARS-CoV-2) (R_0 = 2–5).[2–6] Additionally, a single dose of the live attenuated MeV vaccine has been reported insufficient for acquiring life-long immunity without the boosting effect of natural infection.[7] This issue is exemplified by observed sporadic MeV outbreaks and an increase in global MeV cases by 31% from 2016 to 2017 despite the availability of a MeV vaccine.[8–11] In children under five years of age, measles was responsible for 1.2% of deaths in 2015.[12] Moreover, MeV can cause subacute sclerosing panencephalitis (SSPE) by establishing a chronic, latent infection of the brain.[13,14] Therefore, in addition to vaccination, developing anti-MeV drugs is required to prevent measles outbreaks. Previously, several classes of MeV inhibitors were reported, including peptides, natural extracts, nucleoside derivatives, and small-molecule compounds.[15–17] Small-molecule compounds that target MeV L protein (AS13A, 16677, ERDRP-00519, and GHP-88309) inhibit MeV RNA synthesis.[18,19] However, there are no approved drugs for antiviral therapy against MeV infection.[16,20–22]

MeV has six transcription units, N, P, M, F, H, and L genes, which encode nucleocapsid (N), phospho (P), matrix (M), fusion (F), hemagglutinin (H), and large polymerase (L) proteins. H and F proteins play important roles in the entry step of the life cycle. The H protein binds to host

[1]Department of Infectious Diseases, Tohoku University Graduate School of Medicine, 2-1, Seiryo-machi, Aoba-ku, Sendai, Miyagi 980-8575, Japan
[2]Department of Clinical Laboratory Medicine, Tohoku University Hospital, 1-1, Seiryo-machi, Aoba-ku, Sendai, Miyagi 980-8574, Japan
[3]Graduate School of Pharmaceutical Sciences, Kyoto University, 46-29, Yoshida-Shimo-Adachi-cho, Sakyo-ku, Kyoto 606-8501, Japan
[4]Department of Intelligent Network for Infection Control, Tohoku University Graduate School of Medicine, 2-1, Seiryo-machi, Aoba-ku, Sendai, Miyagi 980-8575, Japan
[5]Division of Infectious Diseases, International Research Institute of Disaster Science, Tohoku University, 2-1, Seiryo-machi, Aoba-ku, Sendai, Miyagi 980-8575, Japan
[6]Division of Biomedical Measurements and Diagnostics, Graduate School of Biomedical Engineering, Tohoku University, 2-1, Seiryo-machi, Aoba-ku, Sendai, Miyagi 980-8575, Japan
[7]Department of Medicinal Chemistry, Kyoto Pharmaceutical University, 1, Misasagi-Shichono-cho, Yamashina-ku, Kyoto 607-8412, Japan
[8]Department of Infectious Diseases, Graduate School of Medicine and Tohoku Medical Megabank Organization, Tohoku University, 2-1, Seiryo-machi, Aoba-ku, Sendai, Miyagi 980-8575, Japan
[9]Lead contact
*Correspondence: hhayashi@med.tohoku.ac.jp
https://doi.org/10.1016/j.isci.2024.108961

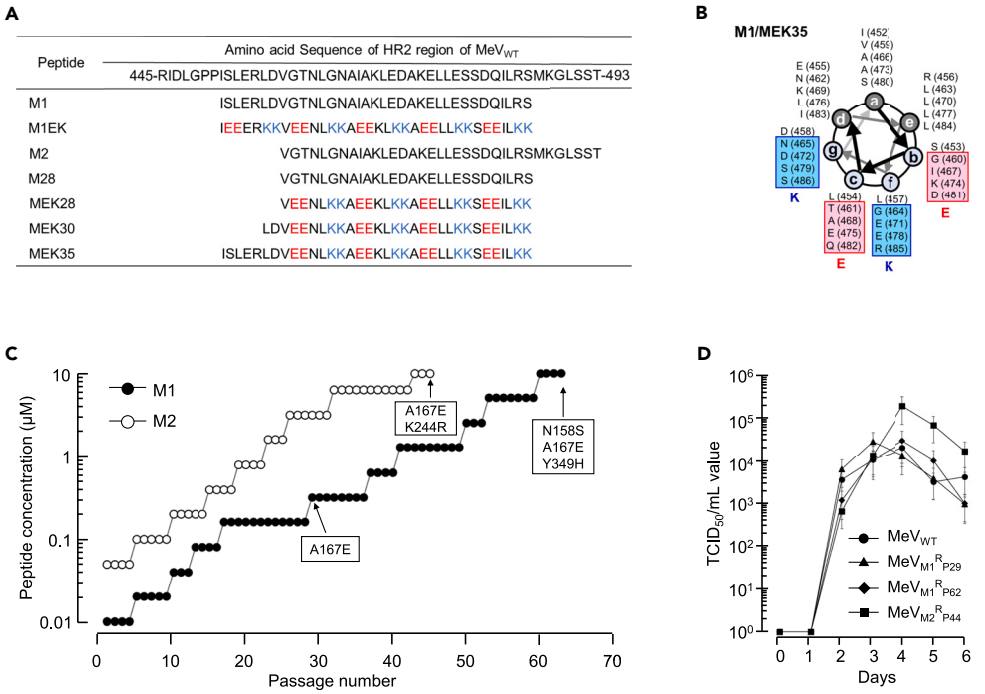

Figure 1. Peptide design and *in vitro* selected M1/M2-resistant MeV variants

(A) Amino acid sequences of the anti-MeV peptides. The amino acid sequence of the HR2 region from a MeV$_{Edm}$ variant is shown at the top of the table as the reference sequence.

(B) Helical wheel representation of M1 and systematic modifications with Glu and Lys to generate MEK35. Light gray positions (b, c, f, and g) form the solvent-exposed surface and dark gray positions (a, d, and e) form the hydrophobic interface.

(C) Results of *in vitro* selection of M1/M2-resistant MeV variants are shown. The MeV$_{Edm}$ variant was passaged in the presence of increasing concentrations of M1 or M2 in B95a cells. The selection for M1 was carried out in a cell-free manner for a total of 63 and 44 passages for M1 and M2, respectively. The concentration of M1 and M2 was initially 0.01 and 0.05 μM, respectively, and gradually increased to 10 μM. Nucleotide sequences of viral RNA were determined using cell lysates of MeV at the indicated (by arrows) passages (passages 29 and 62 for M1 and passage 44 for M2).

(D) Viral infectivity was determined with TCID$_{50}$ values. The infectivity of each MeV variant increased from day 1–2 after inoculation. Only MeV$_{M1}^{R}{}_{p29}$ gave a maximum TCID$_{50}$ value on day 3. The other variants reached maxima on day 4. Data are represented as mean ± SD.

cell receptors, whereas membrane fusion occurs through a conformational change to the F protein. The F protein belongs to the class I viral fusion proteins. The membrane fusion mechanism or conformational change to the F protein is well characterized by two highly conserved heptad repeat (HR) regions, HR1 and HR2, which are important for conformational changes to the F protein. Trimers of HR1 and HR2 interact and form a six-helix coiled-coil bundle (6-HB) that is centered on HR1 and surrounded by HR2.[23,24] Crystal structures of the 6-HB from various viruses have been solved (e.g., respiratory syncytial virus (RSV), human parainfluenza viruses (HPIV), Newcastle disease virus, Nipah virus,[25] SARS-CoV, and SARS-CoV-2).[26,27]

Peptide inhibitors targeting HR1-HR2 interactions can block the conformational change of the class I F protein, thereby inhibiting viral membrane fusion and functioning as a viral fusion inhibitor. These peptide inhibitors can be designed from only amino acids or nucleotide sequence information, as observed for mRNA vaccines. Therefore, peptide inhibitors can be developed rapidly and suppress future unpredictable pandemics by emerging and/or re-emerging viruses by targeting the class I F protein. Peptide-based fusion inhibitors against certain viruses have been reported.[28–31] We have rationally designed peptide-based fusion inhibitors against viruses, which mimic the F protein.[32] In this strategy, peptide-based inhibitors were designed in two steps: (i) the amino acid sequence of the inhibitors was dependent on the well-conserved HR2 of the virus, and (ii) glutamate (E) and lysine (K) substitutions (EK motif) were introduced to solvent-accessible sites of the synthetic peptides. The EK motif retains stable α-helicity and improves pharmacokinetic and pharmacodynamic characteristics.[33,34] Using this strategy, we identified and reported MeV fusion inhibitors, M1, M2, and their derivatives[21,35] (Figure 1). These inhibitors showed high anti-MeV activity *in vitro* (Table 1) and inhibited replication of MeV *in vivo*. There are no data describing resistance to these inhibitors. Acquiring highly M1/M2-resistant MeV variants is crucial for elucidating the mechanism(s) of resistance toward M1 and M2 by MeV and should enable the design of more efficacious and resistance-deferring anti-MeV drugs.

In this report, we generated M1/M2-resistant MeV variants by *in vitro* selection and identified a novel MeV fusion inhibitor, which displayed potent activity against a variant of the MeV Edmonston strain (MeV$_{Edm}$ variant) and M1/M2-resistant MeV populations. Based on the results, we also present an M1 antiviral process that involves three steps: (i) unstructured M1 interacts with the HR1 region; (ii) M1 forms a helical

Table 1. Antiviral activity of peptides against a MeV_{Edm} variant and M1/M2-resistant MeV variants

	EC_{50} (μM) [pEC_{50} ± SD] (fold increase)				
Compounds	MeV_{Edm} variant	$MeV_{M1}{}^{R}{}_{p29}$	$MeV_{M1}{}^{R}{}_{p62}$	$MeV_{M2}{}^{R}{}_{p44}$	CC_{50} (μM)
M1	0.0065 [8.2 ± 0.4]	0.53 [6.3 ± 0.3] (82)	5.9 [5.2 ± 0.2] (908)	0.75 [6.1 ± 0.2] (115)	>10
M1EK	0.15 [6.8 ± 0.7]	>10 [>5] (67)	>10 [>5] (67)	>10 [>5] (67)	>10
M2	0.13 [6.9 ± 0.4]	>10 [>5] (77)	>10 [>5] (77)	>10 [>5] (77)	>10
M28	>10 [>5]	>10 [>5]	>10 [>5]	>10 [>5]	>10
MEK28	0.036 [7.4 ± 0.5]	>10 [>5] (>278)	>10 [>5] (>278)	>10 [>5] (>278)	>10
MEK30	0.013 [7.9 ± 0.5]	0.25 [6.6 ± 0.3] (19)	2.3 [5.6 ± 0.4] (177)	0.20 [6.7 ± 0.2] (15)	>10
MEK35	0.0024 [8.6 ± 0.3]	0.020 [7.7 ± 0.2] (8)	0.028 [7.6 ± 0.2] (12)	0.0084 [8.1 ± 0.4] (4)	>10

Amino acid substitutions identified in the F protein of M1/M2-resistant MeV variants ($MeV_{M1}{}^{R}{}_{p29}$, $MeV_{M1}{}^{R}{}_{p62}$, and $MeV_{M2}{}^{R}{}_{p44}$) when compared to the MeV_{Edm} variant (Edmonston strain) include A167E, N158S/A167E/Y349H, and A167E/K244R, respectively. Numbers in parentheses represent fold changes in EC_{50} values for each variant when compared with the EC_{50} value for MeV_{Edm} variant. All assays were conducted in duplicate, and the data shown represent mean values (±1 standard deviation) of pEC_{50} (log translated EC_{50} value) derived from the results of three to five independent experiments. EC_{50} values were calculated from mean values of pEC_{50}s.

conformation and binds to HR1 through hydrophobic interactions; and (iii) subsequent interactions involving the N-terminal seven amino acids (ISLERLD) or disordered region results in a high-affinity M1-HR1 interaction. Combining the N-terminal seven amino acids and EK motif is important for inhibiting the replication of M1/M2-resistant MeV variants. Thus, a promising factor for peptide-inhibitor design, the combination of disordered and helical conformations, is advocated.

RESULTS

Development of novel fusion inhibitors based on sequence alignment

M1EK, an M1 derivative, showed weaker anti-MeV activity than M1 (Figure 1A; Table 1).[21] There is no crystal structure of 6-HB constructed with HR1 and HR2 of MeV F protein. Nonetheless, sequence alignment of MeV and several viral fusion proteins showed that the amino acid sequences of the HR1 and HR2 domains were highly conserved and formed similar 6-HB structures[26] (Figures S1 and S2). In the 6-HB of viral fusion proteins, the N-terminal region of HR2 is disordered (Figures S1 and S2). The calculated secondary structure of M1 would also have a disordered N-terminal region (Figure S1). In our previous research, we designed M1EK, in which the α-helix-inducible EK motifs were applied to the entire sequence of M1, leading to stabilization of the α-helix structure even at the N-terminal disordered region.[21] However, these different N-terminal structures in M1EK from native M1 might have unfavorable effects on the anti-MeV activity. We designed a series of M1 derivatives (MEK28, MEK30, and MEK35). MEK28 is a 28-residue HR2 peptide consisting of possible α-helix region. MEK30 and MEK35 include a disordered sequence at the N-terminus of MEK28 (Figures 1A and 1B). These derivatives showed stronger anti-MeV activity than M1EK against the MeV_{Edm} variant (Table 1). In particular, MEK35 exerted comparable activity to M1. M28 (a control 28-residue peptide without α-helix-inducible EK motifs) showed no anti-MeV activity.

Effect of the N-terminus on the HR1 inhibitor-binding mode

For structural analysis of HR1-M1 and -M1EK complexes, we built molecular models by using the crystal structures of HPIV3 and RSV 6-HB (PDB: 1ZTM and 3MAW) as starting structures of HR1-M1 and HR1-M1EK complexes, respectively (Figure 2A). The 6-HB structural model of HR1-M1 revealed that three amino acids in the M1 disordered region (I452, E455, and L457) are spatially positioned to form potential hydrogen bonds with S194′, Y181, and N183′, respectively (Figures 2B and 2C). Additionally, L454 of HR2 may be located near a hydrophobic cavity composed of M190′, I187′, and L186 of the F protein. Therefore, the N-terminal disordered region of M1 may interact with amino acids C-terminal of the HR1 region (i.e., L186, I187′, M190′, and S194′). In contrast, the M1 derivative, M1EK, showed reduced interaction with the MeV HR1 trimer (Figures 2D and 2E), supporting the observed weaker anti-MeV activity of M1EK versus M1 (Table 1).

In vitro induction of M1 and M2 resistance

We isolated MeV variants with M1 and M2 resistances by propagating a MeV_{Edm} variant in the presence of the peptides to determine the anti-MeV activity of M1 derivatives against M1/M2 and analyze the mechanism(s) of drug resistance (Figure 1C). B95a cells were inoculated with the MeV_{Edm} variant and cultured in the presence of M1 and M2 at initial concentrations of 0.01 and 0.05 μM, respectively. MeV variants ($MeV_{M1}{}^{R}{}_{p29}$ and $MeV_{M1}{}^{R}{}_{p62}$) replicable in the presence of 0.32 and 10 μM of M1 emerged by passages 29 and 62, respectively (Figure 1C). The MeV_{Edm} variant exposed to M2 by passage 44 ($MeV_{M2}{}^{R}{}_{p44}$) was also replicated in the presence of 10 μM M2. As shown in Table 1, the antiviral activity of M1 decreased against $MeV_{M1}{}^{R}{}_{p29}$, $MeV_{M1}{}^{R}{}_{p62}$, and $MeV_{M2}{}^{R}{}_{p44}$ (EC_{50} values: 0.53, 5.9, and 0.75 μM, respectively). Additionally, M2 lost antiviral

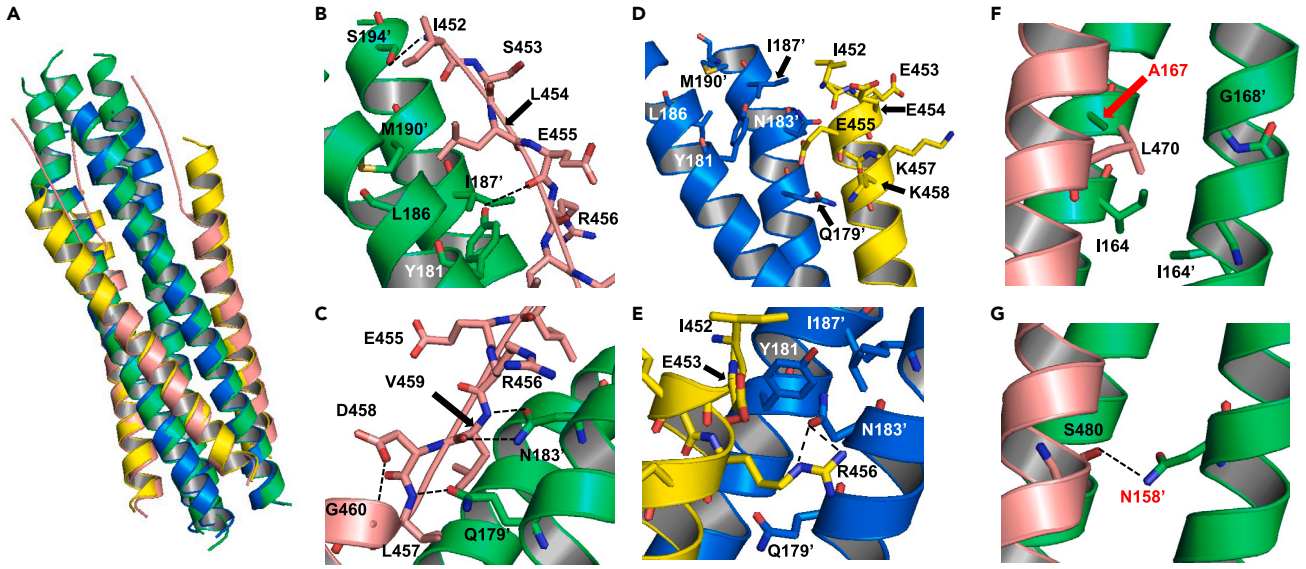

Figure 2. Molecular models of the 6-HB constructed with HR1 and M1 or M1EK

(A) Molecular models of HR1-M1 and HR1-M1EK complexes were superposed. The HR1-M1 complex was built using the 6-HB crystal structure of HPIV3 as the template (PDB: 1ZTM). The HR1-M1EK complex was built using the 6-HB crystal structure of RSV as the template (PDB: 3MAW).

(B) The N-terminus of M1 is shown. The distance between the main-chain nitrogen of I452 and the side-chain oxygen of S194′ is 3.2 Å. Additionally, the distance between the main-chain oxygen of E455 and the side-chain oxygen of Y181 is 3.2 Å, as shown by the black dotted line. L454 of M1 is located in a hydrophobic cavity formed by M190′, I187′, and L186 of HR1.

(C) Amino acid residues around N183′ of HR1. The main-chain oxygen and nitrogen atoms of L457 are proximal to the side-chain nitrogen and oxygen atoms of N183′ (3.2 and 3.5 Å, respectively).

(D) The location of the N-terminal amino acids of M1EK in the 6-HB constructed with HR1 and M1EK.

(E) The side-chain nitrogen atoms of R456 are in close proximity to the side-chain oxygen atom of N183′ (each 2.7 Å).

(F) Amino acid residues surrounding A167 of HR1. L470 of M1 is located near a hydrophobic cavity formed by A167, I164, and G168′ of HR1.

(G) N158′ is in close proximity to S480. The distance between the N158′ and S480 side chains (shown as a black-dashed line) is 3.0 Å.

activity against both *in vitro* selected MeV variants. Thus, the *in vitro* selected MeV variants acquired M1 and M2 cross-resistance (Table 1; Figure S3A).

Sequence analysis of the F protein from *in vitro* selected MeV variants

We analyzed the nucleotide sequence of the F protein coding region of $MeV_{M1}{}^{R}{}_{p29}$, $MeV_{M1}{}^{R}{}_{p62}$, and $MeV_{M2}{}^{R}{}_{p44}$ (Figures 1C and S4). A substitution, A167E, located in the HR1 of MeV, was present in $MeV_{M1}{}^{R}{}_{p29}$. $MeV_{M1}{}^{R}{}_{p62}$ had three substitutions, A167E, N158S, and Y349H, whereas K244R and A167E substitutions were identified in $MeV_{M2}{}^{R}{}_{p44}$. The K244R substitution had a limited effect on M1/M2 resistance because the antiviral activity of M1 against $MeV_{M1}{}^{R}{}_{p29}$ was similar to that against $MeV_{M2}{}^{R}{}_{p44}$. In contrast, the EC_{50} value of M1 against $MeV_{M1}{}^{R}{}_{p62}$ was 908- and 11-fold higher than that against the MeV_{Edm} variant and $MeV_{M1}{}^{R}{}_{p29}$, respectively. These results indicated that in addition to A167E, the mutations N158S and/or Y349H contribute to M1/M2 resistance.

Analyzing the effects of A167E and N157S on HR1-M1 interactions using structure model

The model structure revealed that A167 is located in a hydrophobic cavity with I164, I164′, and G168′ and close to L470 of M1 (Figure 2F), playing an important role in forming hydrophobic interactions between the HR1 trimer and M1. N158 is highly conserved in several viruses (Figure S1). In the structural model, N158 is located at the HR1-M1 interface and may be in proximity to S480 (Figure 2E), similar to the previously reported crystal structures of 6-HBs from several viruses (Figures S1 and S2). The 6-HB structures of these F proteins showed that this conserved asparagine of HR1 forms hydrogen bonds with a serine of HR2, which is also highly conserved in a complementary HR2 region and is located at the same position as S480 of M1 (Figures S1 and S2). Thus, the hydrogen bond between the amine group of MeV-HR1 N158 and the hydroxyl group of M1 S480 would be retained between the hydroxyl groups of MeV-$HR1^{N158S}$ S158 and M1 S480. Therefore, the A167E substitution of the MeV was critical for acquiring M1/M2 resistance.

Effect of A167E and N158S substitutions on HR1-HR2 binding

The sequence analysis showed that M1- and M2-resistant mutations were induced in HR1 (A167E and N158S) but not HR2. To investigate the effect of these mutations on the binding affinity between HR1 and HR2, we established an *in vitro* assay system for detecting the HR1-HR2

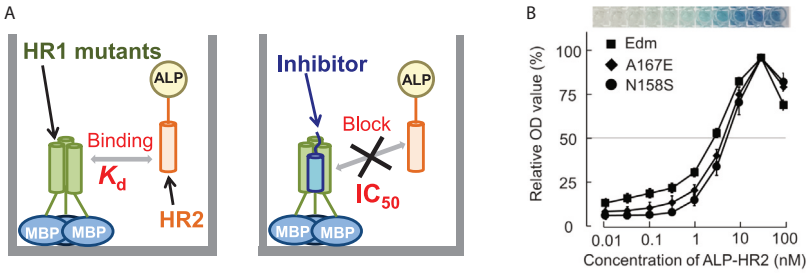

C

	K_d (nM) [pK_d ± SD]	IC_{50} (μM) [pIC_{50} ± SD]	
	HR2	M1	MEK35
$HR1^{Edm}$	2.5 [8.6 ± 0.1]	2.0 [5.7 ± 0.3]	0.026 [7.6 ± 0.3]
$HR1^{A167E}$	4.2 [8.4 ± 0.1]	> 40 [< 4.4]	0.16 [6.8 ± 0.3]
$HR1^{N158S}$	4.9 [8.3 ± 0.1]	2.1 [5.7 ± 0.3]	0.28 [6.5 ± 0.3]

Figure 3. HR1-HR2 binding and inhibition assay

(A) The HR1-HR2 binding and binding inhibition assay. Maltose-binding protein (MBP) fused to HR1 and fixed to 96-well plates binds to alkaline phosphatase (ALP) fused to HR2. The HR1-HR2 interaction is detected by the enzymatic activity of ALP, which is determined by measuring the OD_{630}.

(B) Relative OD_{630} values indicate the interaction between HR2 and HR1 from the MeV_{Edm} variant ($HR1^{Edm}$) or HR1 mutants ($HR1^{A167E}$ and $HR1^{N158S}$).

(C) The dissociation constant (K_d) of the $HR1^{Edm}$ was similar to those of $HR1^{A167E}$ and $HR1^{N158S}$. Binding inhibition activity of M1 and MEK35 against $HR1^{Edm}$, $HR1^{A167E}$, and $HR1^{N158S}$. IC_{50} represents the 50% inhibition concentration and was calculated from mean values of pIC_{50}s (log translated IC_{50}). Data shown represent mean values (±1 standard deviation) of pIC_{50} derived from the results of three to four independent experiments.

interaction (Figures 3A and 3B).[31] The HR1-HR2 binding assay results revealed that the dissociation constants (K_d) of HR2 to HR1 including mutations ($HR1^{A167E}$ and $HR1^{N158S}$) and HR1 from the MeV_{Edm} variant ($HR1^{Edm}$) were similar, indicating that A167E and N158S did not affect the HR1-HR2 interaction, supporting the analysis results using structural modeling (Figures 2G and 3C). Furthermore, the effect of each substitution on the binding affinity of M1 toward $HR1^{A167E}$ and $HR1^{N158S}$ was determined (Figures 3A and 3C). M1 showed a very weak binding affinity toward $HR1^{A167E}$ (IC_{50} > 40 μM), whereas the binding affinity of M1 toward $HR1^{N158S}$ and $HR1^{WT}$ was similar (IC_{50} = 2.0 and 2.1 μM, respectively), suggesting that Y349H plays an important role for M1 resistance.

Viral replication assay

The other substitutions, K244R and Y351H, are located distal from the M1 binding site in HR1. The results of the multistep growth curve in Vero cells showed that the variants and MeV_{Edm} variant had similar viral infectivity, with infectivity increasing after 1 to 2 days and reaching a maximum after 3 to 4 days (Figure 1D). This observation suggests that A167E, K244R, and the combination of N158S and Y349H had minimal effect on viral infectivity or replication.

CD analysis

We used circular dichroism (CD) spectroscopic analysis to determine the effects of the A167E substitution on the interaction between M1 and HR1 of MeV F protein. The structure of M1 was disordered in the absence of HR1, whereas M1EK formed a helix with a positive maximum at 193 nm and two negative maxima at 208 and 222 nm in the CD spectrum (Figure 4A), showing that introducing the EK motif enhanced the helicity of the unbound peptide.[33] In the presence of $HR1^{Edm}$, M1 formed the 6-HB with $HR1^{Edm}$, giving a CD spectrum consistent with helix formation (Figure 4B). These data indicate that, unlike M1EK, M1 forms helix-to-helix interactions with HR1 through a complex process involving conformational changes (Figure 5A). In contrast, the CD spectrum of M1 with $HR1^{A167E}$ contained no signature maxima and minima consistent with helix formation, indicating that the A167E substitution is critical for MeV-acquired resistance to M1. As shown in Figure 2B, the HR1-M1 hydrophobic interaction around L470 of M1 would be destabilized by the negatively charged A167E substitution.

Antiviral activity of novel inhibitors against M1/M2-resistant MeV variants

The anti-MeV activity of several M1 derivatives (M1, M28, MEK28, MEK30, and MEK35) against M1/M2-resistant MeV variants was examined (Figure 1A; Table 1). M28 showed no anti-MeV activity against any MeV variants. MEK28 blocked the replication of the MeV_{Edm} variant but not the M1/M2-resistant MeV variants. MEK30 inhibited the replication of $MeV_{M1}{}^{R}{}_{p29}$ and $MeV_{M2}{}^{R}{}_{p44}$ on the order of 10^{-7} M and showed weak activity against $MeV_{M1}{}^{R}{}_{p62}$. Notably, MEK35 inhibited the replication of $MeV_{M1}{}^{R}{}_{p29}$, $MeV_{M1}{}^{R}{}_{p62}$, and $MeV_{M2}{}^{R}{}_{p44}$ strongly with EC_{50} values on the order of 10^{-8} M (Table 1; Figure S3B). These results are consistent with those of the HR1-HR2 binding assay (Figure 3C) that MEK35 also inhibited the binding of HR2 to $HR1^{A167E}$ and $HR1^{N158S}$ with IC_{50} values on the order of 10^{-7} M, although the binding was slightly weaker than to $HR1^{Edm}$.

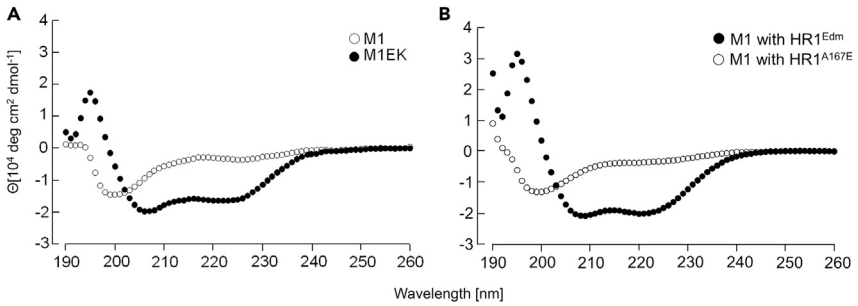

Figure 4. CD spectra of anti-MeV peptides in the absence and presence of $HR1^{Edm}$ or $HR1^{A167E}$

(A) CD spectra of M1 and M1EK in the absence of HR1.

(B) CD spectra of M1 in the presence of $HR1^{Edm}$ and $HR1^{A167E}$.

DISCUSSION

MeV infections were estimated to cause >200,000 mortalities in 2019. Furthermore, some MeV-infected individuals may develop fatal SSPE.[13,36,37] We previously reported fusion inhibitors M1 and derivatives that targeted the HR1 region of the F protein (Figure 1) to suppress MeV infection and showed that these inhibitors exert potent activity *in vitro* and *in vivo*.[21] CD data and structural modeling results herein indicated that M1 underwent conformational changes upon binding to HR1. Furthermore, compared with MEK28, MEK30, and MEK35, the N-terminal extended non-structural region showed stronger activity against the MeV_{Edm} variant. Thus, the N-terminal disordered region (ISLERLD) stabilizes the interaction between HR1 and M1 derivatives. Introducing the EK motif into M1 derivatives at the corresponding part of M28 enhanced helical interactions between the HR1 trimer and M1 derivatives. However, M1, M28, and MEK28 had no antiviral activity against any M1/M2-resistant variants, whereas MEK30 and MEK35 inhibited partially or fully all M1/M2-resistant variants. These results suggest that the antiviral process of M1 involves three steps: (i) unstructured M1 interacts with the HR1 region; (ii) M1 adopts a helical conformation and binds to HR1 through hydrophobic interactions; and (iii) subsequent interactions involving the disordered N-terminal seven amino acids (ISLERLD) give rise to a high-affinity M1-HR1 interaction (Figure 5A). Additionally, the structural model showed that the disordered N-terminal region of M1 and MEK35 interacted with amino acids outside the HR1 region, suggesting that interactions between HR2 and amino acid sequences outside HR1 are also important when designing viral fusion inhibitors. In developing protein-protein or protein-peptide interaction inhibitors, it is important to understand the mechanism of complex formation.[38] On the other hand, peptide inhibitors targeting the class I F protein can be designed based on amino acid sequences in a similar fashion to mRNA vaccine design based on viral nucleic acid sequences, indicating that establishing peptide-design strategies for developing fusion inhibitors should contribute to the prevention and early suppression of future outbreaks by viruses with pandemic potential.[28,29] Peptide inhibitors are difficult to administer orally but can be applied as inhalants for treating and preventing viruses that cause respiratory tract and airborne infections. Additionally, it was reported that direct injection or cholesterol-tagged peptide inhibitors targeting the class I F protein increased penetration of the blood-brain barrier.[21,39] Therefore, peptide inhibitors targeting the MeV F protein are also expected to be suitable as therapeutic agents against SSPE. In contrast, drug prices of peptide-based drugs are typically more expensive than small compound drugs. Solving this problem will require further development of chemical synthesis methods.

The A167E substitution in HR1 introduces minimal steric hindrance in the model structure but likely destabilizes the M1-HR1 hydrophobic interaction, and thus, hampers the stable formation of a helical conformation by M1 (Figure S5). Therefore, binding between the M1/M2-resistant F protein and M1 is unstable. Thus, the A167E substitution inhibits the second step of the proposed M1 antiviral process because destabilizing helix formation hampers the interaction of the N-terminal seven amino acids of M1 with HR1 (Figure 5B). In contrast, in MEK35 with potent activity against $MeV_{M1}{}^{R}{}_{p62}$, the helical conformation downstream of the N-terminal seven amino acids was stabilized by the EK motif (Figure 5C). MEK28 lost antiviral activity against $MeV_{M1}{}^{R}{}_{p29}$ and $MeV_{M1}{}^{R}{}_{p62}$, indicating that the interaction between the helical region of the EK motif and HR1 was destabilized. However, in the cases of MEK30 and MEK35, the N-terminal seven amino acids stabilize binding between the M1/M2-resistant F protein and these derivatives (Figure 5C). Thus, the N-terminal seven amino acids and the EK motif were required to inhibit $MeV_{M1}{}^{R}{}_{p62}$ replication. In contrast, the binding assay results revealed that N158S did not affect the binding affinity of M1 toward HR1 but weakened that of MEK35. In the structural model, N158 of HR1 interacts with S480, which is located at the C-terminus of M1 and MEK35. The different effects of N158S on the binding affinity of M1 and MEK35 may indicate structural differences between the C-terminus of M1 and MEK35. Y349H was shown to be an M1-resistant mutation in the binding assay, but the resistance mechanism is unclear. The structure of the pre-fusion form of the MeV F protein was solved previously.[40] In this structure, three mutations (A167E, N158S, and K244R) are located in a surface region of the F protein. Only Y349H is located at the internal site of the pre-fusion F protein. However, there were no interactions between these mutated amino acids, including Y349H and their adjacent amino acids. Therefore, at least, Y349H affects the post-fusion form and/or structural change process of the MeV F protein. However, further structural research will be required to clarify the roles of Y349H on M1 resistance. Additionally, $MeV_{M2}{}^{R}{}_{p44}$ showed the highest titer in Figure 1D, suggesting that A167E and K244R might affect viral cytopathic and/or replication ability.

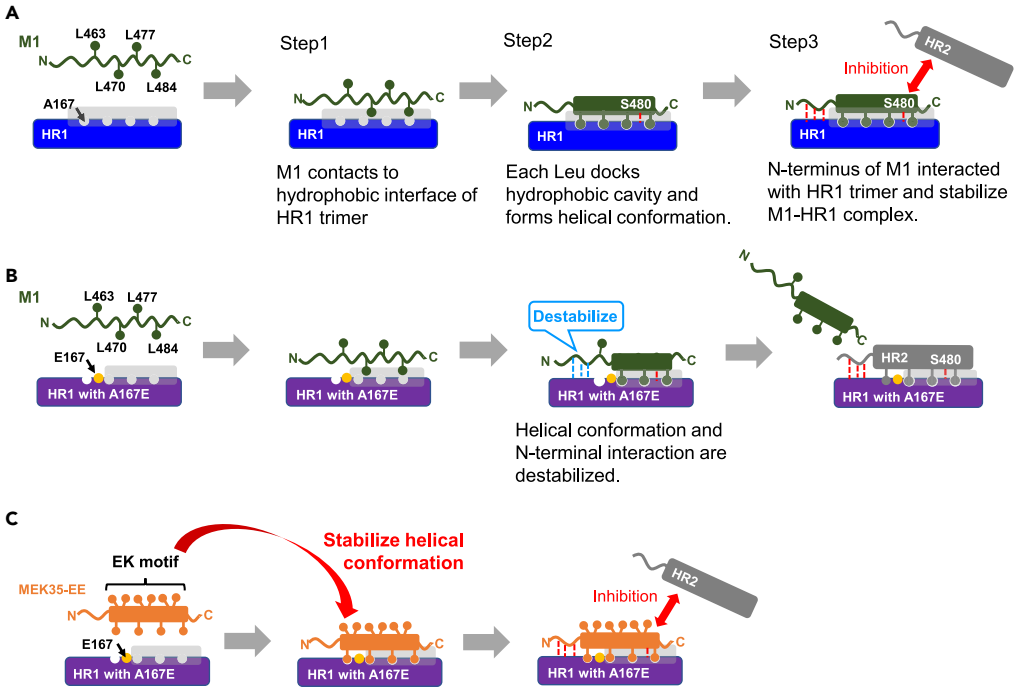

Figure 5. The mechanisms of antiviral activity of HR2-derived peptides against MeV and the development of M1 resistance

(A) Antiviral mechanism of M1 against the MeV_{Edm} variant.

(B) M1-resistant mechanism is illustrated. The A167E substitution inhibits hydrophobic interactions and helix formation around L463 and L470 of M1, destabilizing N-terminal interactions.

(C) The EK motif introduced to MEK35 stabilizes the helical conformation around L463 and L470 and enables the formation of N-terminal interactions.

In conclusion, we demonstrated that MeV acquired M1/M2 resistance by introducing a single substitution, A167E, into the F protein, and MEK35 inhibited M1/M2-resistant MeV strains. Additionally, CD analysis showed that binding between HR1 and M1 was not a simple helix-to-helix interaction but a complex process involving conformational changes. These results provide two important findings: (i) the MeV M1/M2-resistant mechanism and (ii) the importance of both non-helical and helical regions of anti-MeV agents that combat M1/M2-resistant viral strains. Moreover, based on these findings, we proposed a model that describes the antiviral process of M1 (Figure 5). Although the EK motif and stapled peptides[34,41,42] have been presented in several peptide inhibitor designs that focus on helicity,[29] our study advocates a promising factor for peptide-inhibitor design, the combination of non-helical and helical conformations. Additionally, HR1 and HR2 from various viruses have sequential and structural similarities. Indeed, a peptide-based dual fusion inhibitor against HPIV and RSV was designed previously based on structural and sequence similarities of HR2 derived from the fusion protein of each virus.[43] Thus, our findings should aid the development of novel entry inhibitors with high genetic barriers and potent activity against MeV and other viruses with class I F proteins.

Limitations of the study

In this study, MEK35 showed highly potent activity against MeV *in vitro*. We have previously demonstrated that M2 with the EK motif (M2EK) exerts potent activity against SSPE (Yamagata-1 strain) viruses as well as M1 with original sequence and increases the survival rate of SSPE virus-infected mice. Therefore, MEK35 appears to be one of the candidates for therapeutic agents, although it is required further additional preclinical studies, including efficacy and toxicity in appropriate animal models. Moreover, the crystal structure of the post-fusion F protein also remains unknown. Further structural research is required to reveal the mechanisms of the antiviral activity of MEK35 and the drug resistance of MeV.

STAR★METHODS

Detailed methods are provided in the online version of this paper and include the following:

- KEY RESOURCES TABLE
- RESOURCE AVAILABILITY
  - Lead contact
  - Materials availability
  - Data and code availability

SUPPLEMENTAL INFORMATION

Supplemental information can be found online at https://doi.org/10.1016/j.isci.2024.108961.

ACKNOWLEDGMENTS

We are grateful to Kanako Kobayashi for their editorial help. We acknowledge support from the Biomedical Research Core of the Tohoku University Graduate School of Medicine. This work was partly supported by research grants from the Japan Society of the Promotion for Science (JSPS No. JP16H05346, JP18H02555, JP21K19366, and JP23K07918) and by the Joint Usage/Research Center, "Research Center for Zoonosis Control, Hokkaido University. Additionally, this research was supported by AMED under grant numbers JP20ak0101140 and JP22gm1610007 (AMED-CREST). This work was also partly supported by a research grant from the AEON MALL Co. Ltd. We thank Edanz (https://jp.edanz.com/ac) for editing a draft of this manuscript.

AUTHOR CONTRIBUTIONS

Conceptualization, H.H., K.M., S.O., and E.N.K.; methodology, K.H., A.T., S.S., K.K., and H.H.; validation, K.H., A.T., S.M. K.K., M.S.-U., A.N., and M.S.; investigation, K.H., A.T., S.S., K.K., and H.H.; data curation, H.H., E.U., S.O., and E.N.K.; writing – original draft preparation, K.H. and H.H.; writing – review and editing, H.H., E.U., K.M., S.O., and E.N.K.; visualization, K.H., K.M., S.O., and H.H.; supervision, S.O., H.H., and E.N.K.; project administration, H.H., S.O., and E.N.K.; funding acquisition, S.O. and E.N.K.

DECLARATION OF INTERESTS

The authors declare that they have no conflict of interest with the contents of this article.

Received: August 24, 2023
Revised: November 13, 2023
Accepted: January 15, 2024
Published: January 17, 2024

REFERENCES

1. Hersh, B.S., Tambini, G., Nogueira, A.C., Carrasco, P., and de Quadros, C.A. (2000). Review of regional measles surveillance data in the Americas, 1996–99. Lancet *355*, 1943–1948.
2. Anderson, R.M., and May, R.M. (1982). Directly transmitted infections diseases: control by vaccination. Science *215*, 1053–1060.
3. Anderson, R.M., and May, R.M. (1985). Age-related changes in the rate of disease transmission: implications for the design of vaccination programmes. J. Hyg. *94*, 365–436.
4. Ceccarelli, M., Berretta, M., Venanzi Rullo, E., Nunnari, G., and Cacopardo, B. (2020). Editorial–Differences and similarities between Severe Acute Respiratory Syndrome (SARS)-CoronaVirus (CoV) and SARS-CoV-2. Would a rose by another name smell as sweet? Eur. Rev. Med. Pharmacol. Sci. *24*, 2781–2783.
5. Liu, Y., and Rocklöv, J. (2021). The reproductive number of the Delta variant of SARS-CoV-2 is far higher compared to the ancestral SARS-CoV-2 virus. J. Travel Med. *28*, taab124.
6. Organization, W.H. (2003). Strategic Plan for Measles and Congenital Rubella Infection in the European Region of WHO (WHO Regional Office for Europe).
7. Paunio, M., Hedman, K., Davidkin, I., Valle, M., Heinonen, O.P., Leinikki, P., Salmi, A., and Peltola, H. (2000). Secondary measles vaccine failures identified by measurement of IgG avidity: high occurrence among teenagers vaccinated at a young age. Epidemiol. Infect. *124*, 263–271.
8. Paules, C.I., Marston, H.D., and Fauci, A.S. (2019). Measles in 2019—going backward. N. Engl. J. Med. *380*, 2185–2187.
9. Dabbagh, A., Laws, R.L., Steulet, C., Dumolard, L., Mulders, M.N., Kretsinger, K., Alexander, J.P., Rota, P.A., and Goodson, J.L. (2018). Progress toward regional measles elimination—worldwide, 2000–2017. MMWR Morb. Mortal. Wkly. Rep. *67*, 1323.
10. Fukuhara, H., Mwaba, M.H., and Maenaka, K. (2020). Structural characteristics of measles virus entry. Curr. Opin. Virol. *41*, 52–58.
11. Griffin, D.E. (2020). Measles virus persistence and its consequences. Curr. Opin. Virol. *41*, 46–51.
12. Liu, L., Oza, S., Hogan, D., Chu, Y., Perin, J., Zhu, J., Lawn, J.E., Cousens, S., Mathers, C., and Black, R.E. (2016). Global, regional, and national causes of under-5 mortality in

2000–15: an updated systematic analysis with implications for the Sustainable Development Goals. Lancet *388*, 3027–3035.
13. Ikegame, S., Hashiguchi, T., Hung, C.-T., Dobrindt, K., Brennand, K.J., Takeda, M., and Lee, B. (2021). Fitness selection of hyperfusogenic measles virus F proteins associated with neuropathogenic phenotypes. Proc. Natl. Acad. Sci. USA *118*, e2026027118.
14. Schönberger, K., Ludwig, M.-S., Wildner, M., and Weissbrich, B. (2013). Epidemiology of subacute sclerosing panencephalitis (SSPE) in Germany from 2003 to 2009: a risk estimation. PLoS One *8*, e68909.
15. Barnard, D.L. (2004). Inhibitors of measles virus. Antivir. Chem. Chemother. *15*, 111–119.
16. Plemper, R.K., and Snyder, J.P. (2009). Measles control–can measles virus inhibitors make a difference? Curr. Opin. Investig. Drugs *10*, 811–820.
17. Sun, A., Chandrakumar, N., Yoon, J.-J., Plemper, R.K., and Snyder, J.P. (2007). Non-nucleoside inhibitors of the measles virus RNA-dependent RNA polymerase complex activity: synthesis and in vitro evaluation. Bioorg. Med. Chem. Lett. *17*, 5199–5203.
18. Ferren, M., Horvat, B., and Mathieu, C. (2019). Measles encephalitis: towards new therapeutics. Viruses *11*, 1017.
19. Cox, R.M., Sourimant, J., Toots, M., Yoon, J.-J., Ikegame, S., Govindarajan, M., Watkinson, R.E., Thibault, P., Makhsous, N., Lin, M.J., et al. (2020). Orally efficacious broad-spectrum allosteric inhibitor of paramyxovirus polymerase. Nat. Microbiol. *5*, 1232–1246.
20. Plemper, R.K. (2020). Measles resurgence and drug development. Curr. Opin. Virol. *41*, 8–17.
21. Watanabe, M., Hashimoto, K., Abe, Y., Kodama, E.N., Nabika, R., Oishi, S., Ohara, S., Sato, M., Kawasaki, Y., Fujii, N., and Hosoya, M. (2016). A novel peptide derived from the fusion protein heptad repeat inhibits replication of subacute sclerosing panencephalitis virus in vitro and in vivo. PLoS One *11*, e0162823.
22. Ndungu, J.M., Krumm, S.A., Yan, D., Arrendale, R.F., Reddy, G.P., Evers, T., Howard, R., Natchus, M.G., Saindane, M.T., Liotta, D.C., et al. (2012). Non-nucleoside inhibitors of the measles virus RNA-dependent RNA polymerase: Synthesis, structure–activity relationships, and pharmacokinetics. J. Med. Chem. *55*, 4220–4230.
23. Moss, W.J., and Griffin, D.E. (2006). Global measles elimination. Nat. Rev. Microbiol. *4*, 900–908.
24. Rota, P.A., Moss, W.J., Takeda, M., de Swart, R.L., Thompson, K.M., and Goodson, J.L. (2016). Measles. Nat. Rev. Dis. Primers *2*, 16049.
25. Aggarwal, M., and Plemper, R.K. (2020). Structural insight into paramyxovirus and pneumovirus entry inhibition. Viruses *12*, 342.
26. Liu, Y., Xu, Y., Lou, Z., Zhu, J., Hu, X., Gao, G.F., Qiu, B., Rao, Z., and Tien, P. (2006). Structural characterization of mumps virus fusion protein core. Biochem. Biophys. Res. Commun. *348*, 916–922.
27. Xia, S., Liu, M., Wang, C., Xu, W., Lan, Q., Feng, S., Qi, F., Bao, L., Du, L., Liu, S., et al. (2020). Inhibition of SARS-CoV-2 (previously 2019-nCoV) infection by a highly potent pan-coronavirus fusion inhibitor targeting its spike protein that harbors a high capacity to mediate membrane fusion. Cell Res. *30*, 343–355.
28. Outlaw, V.K., Lemke, J.T., Zhu, Y., Gellman, S.H., Porotto, M., and Moscona, A. (2020). Structure-guided improvement of a dual HPIV3/RSV fusion inhibitor. J. Am. Chem. Soc. *142*, 2140–2144.
29. Outlaw, V.K., Cheloha, R.W., Jurgens, E.M., Bovier, F.T., Zhu, Y., Kreitler, D.F., Harder, O., Niewiesk, S., Porotto, M., Gellman, S.H., and Moscona, A. (2021). Engineering protease-resistant peptides to inhibit human parainfluenza viral respiratory infection. J. Am. Chem. Soc. *143*, 5958–5966.
30. Mathieu, C., Porotto, M., Figueira, T.N., Horvat, B., and Moscona, A. (2018). Fusion inhibitory lipopeptides engineered for prophylaxis of Nipah virus in primates. J. Infect. Dis. *218*, 218–227.
31. Nishikawa, H., Kodama, E., Sakakibara, A., Fukudome, A., Izumi, K., Oishi, S., Fujii, N., and Matsuoka, M. (2008). Novel screening systems for HIV-1 fusion mediated by two extra-virion heptad repeats of gp41. Antiviral Res. *80*, 71–76.
32. Nishikawa, H., Nakamura, S., Kodama, E., Ito, S., Kajiwara, K., Izumi, K., Sakagami, Y., Oishi, S., Ohkubo, T., Kobayashi, Y., et al. (2009). Electrostatically constrained α-helical peptide inhibits replication of HIV-1 resistant to enfuvirtide. Int. J. Biochem. Cell Biol. *41*, 891–899.
33. Nishikawa, H., Oishi, S., Fujita, M., Watanabe, K., Tokiwa, R., Ohno, H., Kodama, E., Izumi, K., Kajiwara, K., Naitoh, T., et al. (2008). Identification of minimal sequence for HIV-1 fusion inhibitors. Bioorg. Med. Chem. *16*, 9184–9187.
34. Naito, T., Izumi, K., Kodama, E., Sakagami, Y., Kajiwara, K., Nishikawa, H., Watanabe, K., Sarafianos, S.G., Oishi, S., Fujii, N., and Matsuoka, M. (2009). SC29EK, a peptide fusion inhibitor with enhanced α-helicity, inhibits replication of human immunodeficiency virus type 1 mutants resistant to enfuvirtide. Antimicrob. Agents Chemother. *53*, 1013–1018.
35. Lambert, D.M., Barney, S., Lambert, A.L., Guthrie, K., Medinas, R., Davis, D.E., Bucy, T., Erickson, J., Merutka, G., and Petteway, S.R., Jr. (1996). Peptides from conserved regions of paramyxovirus fusion (F) proteins are potent inhibitors of viral fusion. Proc. Natl. Acad. Sci. USA *93*, 2186–2191.
36. Patel, M.K., Goodson, J.L., Alexander, J.P., Jr., Kretsinger, K., Sodha, S.V., Steulet, C., Gacic-Dobo, M., Rota, P.A., McFarland, J., Menning, L., et al. (2020). Progress toward regional measles elimination—worldwide, 2000–2019. MMWR Morb. Mortal. Wkly. Rep. *69*, 1700.
37. Watanabe, S., Shirogane, Y., Sato, Y., Hashiguchi, T., and Yanagi, Y. (2019). New insights into measles virus brain infections. Trends Microbiol. *27*, 164–175.
38. Hayashi, H., Takamune, N., Nirasawa, T., Aoki, M., Morishita, Y., Das, D., Koh, Y., Ghosh, A.K., Misumi, S., and Mitsuya, H. (2014). Dimerization of HIV-1 protease occurs through two steps relating to the mechanism of protease dimerization inhibition by darunavir. Proc. Natl. Acad. Sci. USA *111*, 12234–12239.
39. Porotto, M., Rockx, B., Yokoyama, C.C., Talekar, A., DeVito, I., Palermo, L.M., Liu, J., Cortese, R., Lu, M., Feldmann, H., et al. (2010). Inhibition of Nipah virus infection in vivo: targeting an early stage of paramyxovirus fusion activation during viral entry. PLoS Pathog. *6*, e1001168.
40. Hashiguchi, T., Fukuda, Y., Matsuoka, R., Kuroda, D., Kubota, M., Shirogane, Y., Watanabe, S., Tsumoto, K., Kohda, D., Plemper, R.K., and Yanagi, Y. (2018). Structures of the prefusion form of measles virus fusion protein in complex with inhibitors. Proc. Natl. Acad. Sci. USA *115*, 2496–2501.
41. Bird, G.H., Mazzola, E., Opoku-Nsiah, K., Lammert, M.A., Godes, M., Neuberg, D.S., and Walensky, L.D. (2016). Biophysical determinants for cellular uptake of hydrocarbon-stapled peptide helices. Nat. Chem. Biol. *12*, 845–852.
42. Madden, M.M., Rivera Vera, C.I., Song, W., and Lin, Q. (2009). Facile synthesis of stapled, structurally reinforced peptide helices via a photoinduced intramolecular 1, 3-dipolar cycloaddition reaction. Chem. Commun. 5588–5590.
43. Outlaw, V.K., Bottom-Tanzer, S., Kreitler, D.F., Gellman, S.H., Porotto, M., and Moscona, A. (2019). Dual inhibition of human parainfluenza type 3 and respiratory syncytial virus infectivity with a single agent. J. Am. Chem. Soc. *141*, 12648–12656.
44. Šali, A., and Blundell, T.L. (1993). Comparative protein modelling by satisfaction of spatial restraints. J. Mol. Biol. *234*, 779–815.
45. Yanagi, Y. (2001). The cellular receptor for measles virus—elusive no more. Rev. Med. Virol. *11*, 149–156.
46. Nakagawara, K., Hayashi, H., Kawaji, K., Sasano, M., and Kodama, E.N. (2020). Application of human lymphoid cells for the evaluation of antivirals against human adenovirus type 19: Zalcitabine has superior activity compared to cidofovir. Antivir. Chem. Chemother. *28*, 2040206620921319.
47. Watanabe, W., Konno, K., Ijichi, K., Inoue, H., Yokota, T., and Shigeta, S. (1994). MTT colorimetric assay system for the screening of anti-orthomyxo-and anti-paramyxoviral agents. J. Virol. Methods *48*, 257–265.
48. Yin, H.-S., Paterson, R.G., Wen, X., Lamb, R.A., and Jardetzky, T.S. (2005). Structure of the uncleaved ectodomain of the paramyxovirus (hPIV3) fusion protein. Proc. Natl. Acad. Sci. USA *102*, 9288–9293.
49. Zhao, X., Singh, M., Malashkevich, V.N., and Kim, P.S. (2000). Structural characterization of the human respiratory syncytial virus fusion protein core. Proc. Natl. Acad. Sci. USA *97*, 14172–14177.

STAR★METHODS

KEY RESOURCES TABLE

REAGENT or RESOURCE	SOURCE	IDENTIFIER
Bacterial and virus strains		
Measles virus	Gift from Dr. Shiro Shigeta (Fukushima Medical University, Japan)	N/A
Biological samples		
BL21-CodonPlus (DE3)-RIL Competent Cells	Agilent Technologies	Cat# 230245
JM109 Competent Cells	NIPPON GENE	Cat# 311-06244
Chemicals, peptides, and recombinant proteins		
Chloramphenicol	Wako	Cat# 034–10572; CAS: 56-75-7
Kanamycin	Meiji Seika	Cat# 6169400A1036; CAS: 8063-07-8
Penicillin G	Meiji Seika	Cat# 6111400D3051; CAS: 69-57-8
Streptomycin	Meiji Seika	Cat# 6161400D1034; CAS: 57-92-1
Experimental models: Cell lines		
B95a cells	Gift from Dr. Suzutani Shigeta (Fukushima Medical University, Japan)	N/A
Vero cells	JCRB Cell Bank (https://cellbank.nibiohn.go.jp/english)	Cat# JCRB0111
Oligonucleotides		
Primers for sequence, See Table S1	This paper	N/A
Primers for cloning, See Table S1	This paper	N/A
Recombinant DNA		
pET47b vector (for expression of alkaline phosphatase- HR2 fusion protein)	Novagen	71461–3
pMAL-c6T vector (for expression of maltose binding protein-HR1 fused protein)	New England Biolabs	N0378S
Software and algorithms		
Modeller	Šali, A. et al.[44]	https://salilab.org/modeller/
Other		
Microplate reader 800TS	Agilent Technologies	https://www.chem-agilent.com/contents.php?id=1006844
Preparative HPLC LC-6AD	Shimadzu	N/A
LC-MS (Alliance e2695/micromass ZQ)	Waters	N/A

RESOURCE AVAILABILITY

Lead contact

Further information and requests for resources should be directed to and will be fulfilled by Hironori Hayashi (hhayashi@med.tohoku.ac.jp).

Materials availability

This study did not generate new materials or reagents.

Data and code availability

All data reported in this paper will be shared by the lead contact upon request.

This paper does not report original code.

Any additional information required the data reported in this paper is available from the lead contact upon request.

EXPERIMENTAL MODEL AND STUDY PARTICIPANT DETAILS

Virus and cell lines

The MeV used in this research was a MeV_{Edm} variant and a kind gift from Dr. Shiro Shigeta (Fukushima Medical University, Japan). The virus stock was prepared by inoculating B95a cells derived from marmoset B lymphoblast cells.[45] Viral titers of each stock solution were 1,400,000 $TCID_{50}$/mL (50% tissue-culture infective dose) for a MeV_{Edm} variant, 300,000 $TCID_{50}$ for $MeV_{M1}{}^{R}{}_{p29}$, 700,000 $TCID_{50}$ for $MeV_{M1}{}^{R}{}_{p62}$ and 800,000 $TCID_{50}$ for $MeV_{M2}{}^{R}{}_{p44}$. The cells were cultured with RPMI-1640 containing 10% fetal calf serum (FCS), 100 unit/mL penicillin G and 50 μg/mL streptomycin (RPMI-FCS). Vero cells derived from the African green monkey kidney were cultured with Dulbecco's Modified Eagle Medium (DMEM) containing 10% FCS, penicillin G (100 unit/mL) and streptomycin (50 μg/mL).

METHOD DETAILS

Peptide synthesis

The peptide resins were manually constructed on NovSynTGR resin (0.25 mmol/g, 0.1 mmol/vessel) using Fmoc-protected amino acids (5 eq.), DIC (5 eq.), HOBt·H_2O (5 eq.) in DMF. Alternatively, the peptide resins were constructed on H-Rink amide ChemMatrix resin (0.5 mmol/g, 0.01 or 0.02 mmol/vessel) or Fmoc-NH-SAL resin (0.45 mmol/g, 0.02 mmol/vessel) by an automatic peptide synthesizer (PSSM-8, Shimadzu) using Fmoc-protected amino acids (5 eq.), HBTU (5 eq.), HOBt·H_2O (5 eq.), and DIEA (10 eq) in DMF (or NMP-DMF for the coupling of Phe). For the side-chain protection, *t*-Bu ester for Asp and Glu; 2,2,4,6,7-pentamethyldihydrobenzofuran-5-sulfonyl (Pbf) for Arg; *t*-Bu for Thr, Tyr and Ser; Boc for Lys; Trt for Gln, and Asn were employed for side-chain protection. Fmoc-protecting group was removed by treatment with 20% piperidine in DMF for 20 min (for manual synthesis) or for 5 min twice (for PSSM-8). Subsequently, the resin was treated with Ac_2O (10 eq.) and pyridine (10 eq.) in DMF. The resulting resin was treated with a cocktail of TFA/H_2O/*m*-cresol/thioanisole/EDT (80:5:5:5:5, ca. 4 mL per 0.02 mmol resin) for 2 h at room temperature. After filtration, cold Et_2O was added to the filtrate. The resulting precipitate was washed with cold Et_2O (50 mL) twice. The resulting crude peptide was purified by RP-HPLC on a Cosmosil 5C18 AR-300 (Nacalai Tesque Inc., Kyoto, Japan, 20 × 250 mm) with a linear gradient of CH_3CN containing 0.1% TFA at a flow rate of 8 mL/min to provide the expected peptides as the TFA salt. All peptides were characterized by ESI-MS (micromass ZQ, Waters) and purity was calculated as >95% by HPLC.

MEK28: 47.0 mg from 0.05 mmol resin (NovaSynTGR resin). LRMS (ESI+) calcd for $C_{150}H_{265}N_{39}O_{47}$: 3367.00. Observed *m/z*: $[M+5H]^{5+}$: 674.43: $[M+4H]^{4+}$: 842.87; $[M+3H]^{3+}$: 1123.60.

M28: 4.2 mg from 0.02 mmol resin (H-Rink amide ChemMatrix resin). LRMS (ESI+) calcd for $C_{129}H_{221}N_{37}O_{46}$: 3026.40. Observed *m/z*: $[M+3H]^{3+}$: 1009.89; $[M+2H]^{2+}$: 1514.67.

MEK30: 21.4 mg from 0.04 mmol resin (Fmoc-NH-SAL resin). LRMS (ESI+) calcd for $C_{160}H_{281}N_{41}O_{51}$: 3595.24. Observed *m/z*: $[M+5H]^{5+}$: 720.22; $[M+4H]^{4+}$: 900.10; $[M+3H]^{3+}$: 1199.85.

MEK35: 18.1 mg from 0.04 mmol resin (Fmoc-NH-SAL resin). LRMS (ESI+) calcd for $C_{186}H_{327}N_{49}O_{59}$: 4193.95. Observed *m/z*: $[M+5H]^{5+}$: 839.96; $[M+4H]^{4+}$: 1049.77; $[M+3H]^{3+}$: 1399.24.

HR1^{WT} [Ac-QAIDNLRASLETTNQAIEAIRQAGQEMILAVQGVQDYINN-NH_2]: 11.9 mg from 0.02 mmol resin (H-Rink amide ChemMatrix resin). LRMS (ESI+) calcd for $C_{188}H_{311}N_{57}O_{65}S$: 4441.95. Observed *m/z*: $[M+4H]^{4+}$: 1111.41; $[M+3H]^{3+}$: 1481.34.

HR1^{A167E} [Ac-QAIDNLRASLETTNQAIEAIRQEGQEMILAVQGVQDYINN-NH_2]: 13.2 mg from 0.04 mmol resin (H-Rink amide ChemMatrix resin). LRMS (ESI+) calcd for $C_{190}H_{313}N_{57}O_{67}S$: 4499.99. Observed *m/z*: $[M+4H]^{4+}$: 1126.04; $[M+3H]^{3+}$: 1501.07.

Generation of M1-and M2-resistant MeV *in vitro*

B95a cells (2.0 × 10^5 cells/mL) were exposed to the MeV_{Edm} variant and cultured in the presence of M1 and M2 at 10 and 50 nM, respectively. Viral replication was monitored by visually observing the cytopathic effects of the virus. The culture supernatants were harvested at 3 to 5 days and used to infect fresh B95a cells for the next round of culturing in the presence of increasing concentrations of each peptide. The peptide concentrations were increased 2-fold when the virus began to replicate well in the presence of the peptides. Viral RNA samples obtained from the supernatant of cell cultures were subjected to nucleotide sequencing. This selection procedure was carried out until the peptide concentration reached 10 μM.

Sequence analysis

Viral RNA was extracted from harvested MeV variants using the TRI Reagent (Sigma-Aldrich, St Louis, MO, USA). The viral RNAs were then subjected to reverse transcription coupled (RT)-PCR using PrimeScript One-Step RT-PCR Kit Ver. 2 (Takara Bio, Shiga, Japan). The RT-PCR products were purified using ExoSAP-IT (Thermo Fisher Scientific, Waltham, MA, USA). Sequence reactions were performed using Big Dye Terminator (Applied Biosystems, Foster City, CA, USA). The primer sets for RT-PCR and sequence reactions are listed in Table S1.

Antiviral activity and cell cytotoxicity assay

Each compound was added to a 96-well plate and serially diluted 10-fold using RPMI-FCS to give concentrations between 0.01 and 10 μM. After serial dilution, MeV and B95a cells (2 × 10^4 cells/well) were added to the plate. The plates were incubated for 8 days at 37°C and in the presence of 5% CO_2. Cell viability was determined at the end of the incubation period using the MTT assay, as described previously.[46,47] The 50% antiviral effective concentration (EC_{50}) was defined as the drug concentration that protects 50% of the virus-infected cells from virus-induced cell damage and/or death. The cytotoxicity of each compound was measured using the same method as the

EC_{50} in the absence of the MeV. The 50% cytotoxicity concentration (CC_{50}) is the drug concentration that reduces cell viability by 50%. Data shown represent mean EC_{50} and CC_{50} values (±1 standard deviation) derived from the results of three to four independent experiments conducted in duplicate.

Construction of the protein expression vectors

As mentioned, HR1 and HR2 DNA fragments were amplified from viral RNA using RT-PCR. The DNA fragment of the ALP coding region without the secretory signal sequence (residues 22–471) was amplified by PCR from the *E. coli* JM109 genome (K12 strain, ECOS JM109, NIPPON GENE). The amplified DNA fragment was inserted into the pET47b vector (Novagen, Billerica, MA, USA) using *Bam*HI and *Hind*III (pET-ALP vector). HR2 DNA was then inserted into the pET-ALP vector using *Hind*III and *Xho*I (pET-ALP-HR2). HR1 DNA was inserted into the pMAL-c6T vector (NEB, Ipswich, MA, USA) using *Sal*I and *Bam*HI (pMAL-HR1), as described previously, with some modifications.[31] Primer sequences using vector cloning are listed in Table S1.

Protein expression and purification

Each constructed vector was transformed into *E. coli* BL21-Codon Plus (DE3)-RIL cells (Agilent Technologies, Santa Clara, CA, USA) by heat-shock transformation. The culture was grown in a shake flask containing Luria broth plus ampicillin or kanamycin and chloramphenicol ($LB^{Am+/Cp+}$ for pMAL-HR1 and $LB^{Km+/Cp+}$ for pET-ALP-HR2) at 37°C. The LB culture was grown in flasks at 37°C to an optical density of 0.6 at 600 nm, and the expression of each protein was induced by the addition of isopropyl β-D-thiogalactopyranoside (1.0 mM for MBP-HR1 and 0.3 mM for ALP-HR2). MBP-HR1 was expressed for 4 h at 37°C. ALP-HR2 was expressed for 10 h at 25°C. After culturing, the cells were harvested by centrifugation, and the obtained cell pellets were stored at −80°C until use. For purification of MBP-HR1 and ALP-HR2, each cell pellet was resuspended in 10 mM Tris pH 8.0 and lysed by sonication. The cell lysates were separated into supernatant and inclusion body fractions by centrifugation. Each fusion protein was confirmed to be present in the supernatant fraction. MBP-HR1 and ALP-HR2 were purified using Amylose Resin (NEB) and Ni-NTA Agarose (QIAGEN, Hilden, Germany), respectively.

HR1-HR2 binding assay

MBP-HR1 was diluted to 50 nM in 50 mM sodium carbonate buffer (pH 9.4) and coated onto a 96-well ELISA plate (Costar 1 × 8 Stripwell high binding EIA/RIA plate, flat bottom, without lid; Corning, New York, NY, USA) overnight at 4°C. Plates were washed three times with PBS containing 0.025% Tween 20 (T-PBS) (pH 7.4), and the plate was then coated with 0.1% bovine serum albumin (BSA) in T-PBS at 4°C for 2.5 h. The wells were washed three times with T-PBS. ALP-HR2 in 100 mM HEPES buffer (pH 7.0) containing 100 mM NaCl and 2 mM $MgCl_2$ was added to the plate and diluted in order. The plate was incubated at 37°C for 1.5 h and washed three times with 100 mM HEPES buffer (pH 7.0) containing 0.025% Tween 20. Phosphatase substrate 5-bromo-4-chloro-3-indolyl phosphate (BCIP) (BluePhos Microwell Phosphatase Substrate; SeraCare Life Sciences, Milford, MA, USA) containing 1 mM $Zn(CH_3COO)_2$ and 2 mM $MgCl_2$ was added and incubated at 37°C for 1 h. The optical density at 630 nm (OD_{630}) was measured by a plate reader (microplate reader 800TS, Bio Tek, Agilent Technologies). The relative OD_{630} value was calculated as a ratio of the OD_{630} value at each drug concentration and the saturated OD_{630} value. The log-transformed dissociation constants (pK_d) were calculated by approximating the two concentrations sandwiching 50% with the following equation: $pK_d = -(LOG(A/B)*(50 - C)/(D - C) + LOG(B))$, where A and B are the high and low concentrations sandwiching 50%. C and D represent the relative OD_{630} values at B and A, respectively. The arithmetic mean of the pK_d values was transformed to K_d values, as presented in the tables and figures.

HR1-HR2 binding inhibition assay

MBP-HR1 (20 nM) and BSA were coated onto a 96-well ELISA plate, as described above. The drug candidates in 100 mM HEPES buffer (pH 7.0) containing 100 mM NaCl and 2 mM $MgCl_2$ were added to the plate and diluted in order. The plate was incubated at 37°C for 1 h. After incubation, ALP-HR2 (10 nM) in the same buffer was added to the plate and incubated at 37°C for 1 h. The plate was washed thrice with 100 mM HEPES buffer (pH 7.0) containing 0.025% Tween 20. BCIP/NBT containing 1 mM $Zn(CH_3COO)_2$ and 2 mM $MgCl_2$ was added and incubated at 37°C for 2 h. The OD_{630} was measured by the plate reader. The relative OD_{630} value was calculated as the ratio of the OD_{630} value at each drug concentration and the highest OD_{630} value. The log-transformed 50% inhibition concentration (pIC_{50}) was defined as the concentration of peptide at which the relative OD_{630} value was 50% and was calculated by approximating the two concentrations sandwiching 50% with the following equation: $-(LOG(A/B)*(50 - C)/(D - C) + LOG(B))$. A, B, C and D were defined above. The arithmetic mean of the pIC_{50} was transformed to IC_{50} values.

Circular dichroism (CD) measurements

CD measurements were performed using a JASCO J-720 or JASCO J-820 circular dichroism spectrometer with a thermoelectric temperature controller (Jasco International Co., Ltd., Tokyo, Japan). A stock solution of each peptide was prepared by dissolving the peptide in TFE at a concentration of 0.5 mM. For CD measurements of a 1:1 mixture of the HR1 peptide and HR2-derived peptide, the concentration of the mixed peptide stock solution was diluted to a final concentration of 10 μM with PBS (pH 7.4) and incubated at 37°C for 30 min. The wavelength-dependent molar ellipticity [θ] was monitored at 25°C as the average of four scans, and the thermal stability of the HR1 and HR2 mixture was estimated by monitoring the change in the CD signal at 222 nm.

Viral replication kinetics assay

Vero cells (1×10^4 cells/well) were inoculated with $10^2 \times TCID_{50}$ of each variant, which was propagated in B95a for 12 h, and then the culture media was replaced with DMEM containing 1% FCS, 100 unit/mL penicillin G and 50 μg/mL streptomycin (DMEM-FCS). The MeV-infected cells were incubated for 6 days, and the culture medium, including viruses, was collected every 24 h. The collected viruses were stored at −80°C until use. To determine the replication kinetics of the MeV mutants, $TCID_{50}$ values of virus stocks, which were collected at each time point, were analyzed by the plaque assay using Vero cells. Each collected virus was added to the 96-well plate and serially diluted 5-fold using DMEM-FCS in the plate. Vero cells (1×10^4 cells/well) were added to the serially diluted viruses and were incubated for 7 to 10 days. The $TCID_{50}$ was calculated by observation of the viral cytopathic effect using a microscope (OLYMPUS, Tokyo, Japan).

Homology modeling of helix bundle structures

For structural modeling, sequence alignments were performed between the MeV HR1 region and M1 peptide (HR1-M1), the HR1 region and M1EK peptide (HR1-M1EK) and the HR1 A167E mutant and MEK35 peptide ($HR1^{A167E}$-MEK35). The binding groove for HR2 peptide consists of two HR1 helices. The helix bundle homology models were built using Modeller using a standard protocol.[44] The human parainfluenza 3 virus structure (PDB: 1ZTM)[48] was used as the template structure for building the HR1-M1 and $HR1^{A167E}$-MEK35 models. The model structure of HR1-M1EK was built using the human RSV structure (PDB: 1G2C)[49] as the template in which a helical structure was theoretically rebuilt for the N-terminal sequence. The binding groove for HR2 peptide consists of two HR1 helices. The prime symbol (′) indicates the residue number of an alternative HR1 sequence on the groove.